tional data underscores the need for major revisions of Jovian models beyond features connected to the molecular H_2 EOS or suggests that reanalysis of the free oscillation observations is required.

REFERENCES AND NOTES

1. H. K. Mao and R. J. Hemley, *Am. Sci.* **80**, 234 (1992).
2. V. N. Zharkov, *Interior Structure of the Earth and Planets* (Harwood, New York, 1986).
3. M. Podolak, W. B. Hubbard, J. B. Pollack, in *Protostars and Planets III*, E. H. Levy and J. I. Lunine, Eds. (Univ. of Arizona Press, Tucson, AZ, 1993), p. 1109.
4. B. Mosser, F. X. Schmider, Ph. Delache, D. Gautier, *Astron. Astrophys.* **251**, 356 (1991); B. Mosser *et al.*, *ibid.* **267**, 604 (1993).
5. J. Provost, B. Mosser, G. Berthomieu, *ibid.* **274**, 595 (1993).
6. W. Hayes and R. Loudon, *Scattering of Light by Crystals* (Wiley, New York, 1978).
7. A. Polian, in *Frontiers of High Pressure Research*, H. D. Hochheimer and R. D. Etters, Eds. (Plenum, New York, 1991), p. 181.
8. H. K. Mao *et al.*, *Science* **239**, 1131 (1988).
9. H. K. Mao *et al.*, *Phys. Rev. Lett.* **60**, 2649 (1988); W. L. Vos *et al.*, *Nature* **358**, 46 (1992).
10. R. J. Hemley *et al.*, *Phys. Rev. B* **42**, 6458 (1990).
11. J. Hu, H. K. Mao, J. F. Shu, R. J. Hemley, in *High Pressure Science and Technology–1993*, S. C. Schmidt, J. W. Shaner, G. A. Samara, M. Ross, Eds. (American Institute of Physics, New York, in press).
12. V. V. Matveev, I. V. Medvedeva, V. V. Prut, P. A. Suslov. S. A. Shibaev, *Pis'ma Zh. Eksp. Teor. Fiz* **39**. 219 (1984): V. P. Glazkov *et al.*, *ibid.* **47**, 661 (1988): J. van Straaten and I. F. Silvera, *Phys. Rev. B* **37**. 1989 (1988).
13. Pure hydrogen gas and a grain of ruby were loaded into a 150-μm hole in a rhenium gasket of a large-aperture diamond cell. A number of Brillouin spectra were recorded in the fluid phase between 1.5 and 4.9 GPa. A new sample was then loaded and carefully pressurized above the room-temperature freezing point (5.4 GPa) to form a single crystal. Pressures were measured from the frequency shift of the R_1 fluorescence line of ruby [H. K. Mao, J. Xu, P. M. Bell, *J. Geophys. Res.* **91**, 4673 (1986)]. The number of crystals and their orientation were determined at each pressure by synchrotron x-ray diffraction at beamline X17C of the National Synchrotron Light Source, Brookhaven National Laboratory. Brillouin scattering measurements were carried out with a newly constructed spectrometer utilizing a six-pass tandem Fabry-Perot interferometer [R. Mock, B. Hillebrands, J. R. Sandercock, *J. Phys. E.* **20**, 656 (1987)]. A single-frequency Ar^+ laser served as the excitation source. The system was designed to allow for a number of different scattering geometries. Most of the data were collected with use of a 90° geometry. Other data were collected in a backscattering geometry, which is sensitive to the product of refractive index and velocity. Further experimental details are presented elsewhere (*34*).
14. R. L. Mills, D. H. Liebenberg, J. C. Bronson, L. C. Schmidt, *J. Chem. Phys.* **66**, 3076 (1977); E. M. Brody, H. Shimizu, H. K. Mao, P. M. Bell, W. A. Bassett, *J. Appl. Phys.* **52**, 3583 (1981).
15. The Brillouin and crystallographic data were inverted with use of Christoffel's equation to obtain the five independent elastic constants of hexagonal H_2. The adiabatic bulk and shear moduli were obtained by orientationally averaging the individual constants. The isothermal bulk modulus was computed from the adiabatic value by making a small thermodynamic correction. The EOS was calculated by integrating over the isothermal bulk modulus (*34*).
16. H. Shimizu, E. M. Brody, H. K. Mao, P. M. Bell, *Phys. Rev. Lett.* **47**, 128 (1981).
17. I. F. Silvera and V. V. Goldman, *J. Chem. Phys.* **69**, 4209 (1978).
18. M. Ross, F. H. Ree, D. A. Young, *ibid.* **79**, 1487 (1983).
19. M. van Thiel *et al.*, *Phys. Earth Planet. Int.* **9**, 57 (1974); R. D. Dick and G. I. Kerley, *J. Chem. Phys.* **73**, 5264 (1980); W. J. Nellis, A. C. Mitchell, M. van Thiel, G. J. Devine, R. J. Trainor, *ibid.* **79**, 1480 (1983).
20. G. Chabrier, D. Saumon, W. B. Hubbard, J. I. Lunine, *Astrophys. J.* **391**, 817 (1992).
21. W. B. Hubbard and M. S. Marley, *Icarus* **78**, 102 (1989).
22. T. V. Gudkova, V. N. Zharkov, V. V. Leont'ev, *Solar Sys. Res.* **22**, 159 (1989); V. N. Zharkov and T. V. Gudkova, *Ann. Geophysicae* **9**, 357 (1991).
23. The potential, ϕ, describes effective isotropic pair-wise interactions and includes many-body terms implicitly. It is based on the form (*17*)
$$\phi(r) = \exp(\alpha - \beta r - \gamma r^2) - \left(\frac{C_6}{r^6} + \frac{C_8}{r^8} + \frac{C_{10}}{r^{10}}\right) f(r) + \frac{C_9}{r^9} f(r)$$
where $f(r)$ is a damping function given by
$$f(r) = \exp\left[- \left(\frac{1.28 r_m}{r} - 1\right)^2 \right] \qquad r < 1.28 r_m$$
$$= 1.0 \qquad r > 1.28 r_m$$
where r is the intermolecular spacing, r_m is the position of the potential well minimum, and the other parameters are constants. The potential also includes a short-range term of the form
$$V_{SR} = a_1 (r - r_c)^3 + a_2 (r - r_c)^6 \qquad r \leq r_c$$
$$= 0 \qquad r > r_c$$
The parameters of the short-range term are as follows: $a_1 = 4.213 \times 10^{-4}$ hartree/bohr³, $a_2 = -8.045 \times 10^{-5}$ hartree/bohr⁶, with $r_c = 5.2912$ bohr. Values of the other parameters are given in (*17*). We emphasize that this is an effective potential for both the solid and fluid phases. Alternatively, one could develop effective potentials appropriate for the two phases (state-dependent potentials). These could differ as a result of possible differences in intermolecular interactions in the two phases, in particular when comparing the room-temperature solid and the shocked fluid (that is, owing to differences in rotational and vibrational excitations). Despite this, we find that the potential provides a very good fit to all high-pressure data (Figs. 1 and 2). Additional constraints on the potential could be obtained from temperature measurements along the Hugoniot (W. J. Nellis, personal communication).
24. Hugoniot curves were calculated by the method described in (*18*), except that dissociation was not included in the calculation.
25. D. J. Stevenson, *Icarus* **62**, 4 (1985).
26. M. Ross, *J. Chem. Phys.* **71**, 1567 (1979). No dissociation was allowed in the adiabat calculations. See (*18*) and (*27*) for additional details and discussion.
27. D. Saumon and G. Chabrier, *Phys. Rev. A* **44**, 5122 (1991); *ibid.* **46**, 2084 (1992).
28. R. Le Toullec, P. Loubeyre, J.-P. Pinceaux, *Phys. Rev. B* **40**, 2368 (1989); A. Polian and M. Grimsditch, *Europhys. Lett.* **2**, 849 (1986).
29. W. Heller, *J. Phys. Chem.* **69**, 1123 (1965); H. Craig, *Geochim. Cosmochim. Acta* **56**, 3001 (1992).
30. L. C. van den Bergh and J. A. Schouten, *J. Chem. Phys.* **89**, 2336 (1988).
31. J. P. Watt, G. F. Davies, R. J. O'Connell, *Rev. Geophys. Space Phys.* **14**, 541 (1976); H. T. Hammel, *Phys. Chem. Liq.* **14**, 171 (1985).
32. D. Gautier and T. Owen, in *Origin and Evolution of Planetary Atmospheres*, S. K. Atreya, J. B. Pollack, M. S. Matthews, Eds. (Univ. of Arizona Press, Tucson, AZ, 1989), p. 487.
33. B. Conrath, D. Gautier, R. Hanel, G. Lindal, A. Marten, *J. Geophys. Res.* **92**, 15003 (1987); E. Anders and N. Grevesse, *Geochim. Cosmochim. Acta* **53**, 197 (1989).
34. C. S. Zha, T. S. Duffy, R. J. Hemley, H. K. Mao, *Phys. Rev. B* **48**, 9246 (1993).
35. R. Wanner and H. Meyer, *J. Low Temp. Phys.* **11**, 715 (1973); P. J. Thomas, S. C. Rand, B. P. Stoicheff, *Can. J. Phys.* **56**, 1494 (1978).
36. F. H. Ree, in *Simple Molecular Systems at Very High Density*, A. Polian, P. Loubeyre, N. Boccara, Eds. (Plenum, New York, 1989), p. 153.
37. These results are consistent with another recent analysis of the data in (*7*) (P. Loubeyre, personal communication).
38. We thank J. F. Shu and J. Z. Hu for assistance in the x-ray diffraction measurements and M. S. Marley, D. Saumon, and P. Loubeyre for useful correspondence. We are also grateful to M. Ross, W. J. Nellis, D. Saumon, and A. Boss for comments and discussion. Supported by NSF and NASA.

29 October 1993; accepted 3 February 1994

Short-Lived Chemical Heterogeneities in the Archean Mantle with Implications for Mantle Convection

Janne Blichert-Toft and Francis Albarède

The neodymium isotope and samarium-neodymium systematics of 2.7-billion-year-old mantle-derived magmas indicate that the lifetime of chemical heterogeneities was much shorter in the Archean mantle than in the modern mantle. Isotopic evidence is compatible with a Rayleigh number 100 times larger and convection 10 times faster in the Late Archean compared with the present-day mantle. Modern plate tectonics thus may be an improbable analog for the Archean. Chemical heterogeneities in the mantle may originate upon magma migration and mineralogical phase changes rather than by recycling of oceanic and continental crust.

The extent of mantle heterogeneity in Archean time is considerably more elusive than that in the modern mantle. Preservation of pre-Phanerozoic mid-ocean ridge basalts is uncertain, and other mantle-derived rocks in the Archean, such as komatiites and continental basalts, may have been contaminated by crustal material (*1*). In addition, the resolution of isotopic data is, from the nature of radiogenic decay, smaller in the Archean than at present.

The development of isotopic heterogeneities in basalts from fractionated radioactive-radiogenic pairs requires that parts of the mantle were isolated for periods of time in excess of 1 billion years (2). Models of mantle convection, however, suggest that on such a time scale, large heterogeneities (≥ 100 km) can hardly survive convective stirring (3, 4). Numerous apparent isotopic ages of 1 to 2 billion years recorded in basalts therefore may reflect the competing effects of continuous heterogeneity creation by mantle melting and their subsequent destruction by convective stirring (5). If the convective state of the Earth has changed with time, presumably through loss of primordial heat and decay of heat-producing elements, a significantly shorter time scale and thereby much smaller isotopic heterogeneities can be expected for Archean mantle-derived rocks.

We examined the isotopic variability of the Archean mantle and compared it to that of the mantle today. The variety of isotopic tracers used to identify components in the modern mantle cannot be adequately applied for ancient rocks. The Rb-Sr and U-Pb isotope pairs each include at least one element that is mobile under subsurface conditions, and not enough Lu-Hf data exist yet for either Archean or modern rocks to afford statistically significant information. The assessment of mantle heterogeneities in the Archean therefore rests solely on the Sm-Nd isotope system. While the isotopic composition of Nd is a robust indicator of the state of relative depletion or enrichment of the mantle source integrated over long periods of time, the Sm/Nd ratio, which is well behaved and widely available, provides the same information at the time of eruption. A potential disadvantage is that for small degrees of melting, the Sm/Nd ratio of basalts may not be identical to that of their source.

Because the largest Sm-Nd isotopic database for the Archean is for rocks of Late Archean age, we focused on the Archean mantle at 2.7 billion years ago (Ga). Combined Nd isotope compositions and Sm and Nd concentrations are available for some 270 Late Archean (2.6- to 2.8-Ga) samples of potential mantle origin. Because the comparison of Archean to modern mantle-derived rocks can provide a biased picture of the ancient mantle heterogeneities if some critical rock groups, such as sea-floor basalts, are missing from the geological record, we examined a wide range of Late Archean rocks with potential mantle affinity, including basalts, komatiites, gabbros, and amphibolites. For the modern mantle, we included only ocean island, mid-ocean ridge, and back-arc basin basalts (OIB, MORB, and BABB). Although several thousand Nd isotope analyses have been published for modern oceanic basalts, Sm and Nd concentrations are not systematically available. In this report, we consider about 1350 samples. Oceanic plateau basalts, which may represent an important protolith for both modern (6) and Precambrian crust (7), are not included in the compilation, but examination of the available data (8) shows overlap with other oceanic basalts.

Density diagrams of the compiled data for both the Late Archean (Fig. 1A) and modern mantle (Fig. 1B) show an overall positive correlation between $\epsilon_{Nd}(T)$ [the part in 10^4 difference in the isotopic composition of Nd between the sample and the CHUR (chondritic uniform reservoir) reference as a function of age T] and $^{147}Sm/^{144}Nd$ for positive $\epsilon_{Nd}(T)$ values. This correlation is particularly striking when all modern basalts are lumped together (Fig. 1B) and when the MORB subset is considered alone (Fig. 1C). By contrast, most modern OIB display a fairly restricted range of $^{147}Sm/^{144}Nd$ ratios (0.12 to 0.15) (Fig. 1D), despite a large spread in $\epsilon_{Nd}(T)$ values.

Because variations in ϵ_{Nd} must reflect compositional variations in the mantle as well as the time intervals during which individual domains remained isolated, the fact that the Sm/Nd ratio correlates with ϵ_{Nd} is prima facie evidence that variations in the former primarily reflect Sm/Nd variations in the mantle and not fractionation during melting. Some additional variability in Sm/Nd, as reflected by the horizontal spread of about 0.05 units in the $^{147}Sm/^{144}Nd$ ratio at constant ϵ_{Nd} (Fig. 1B), undoubtedly is produced by variations in the degree of partial melting, but this effect is subordinate and only accounts for some of the scatter about the general correlation.

The lower limb of Archean mantle

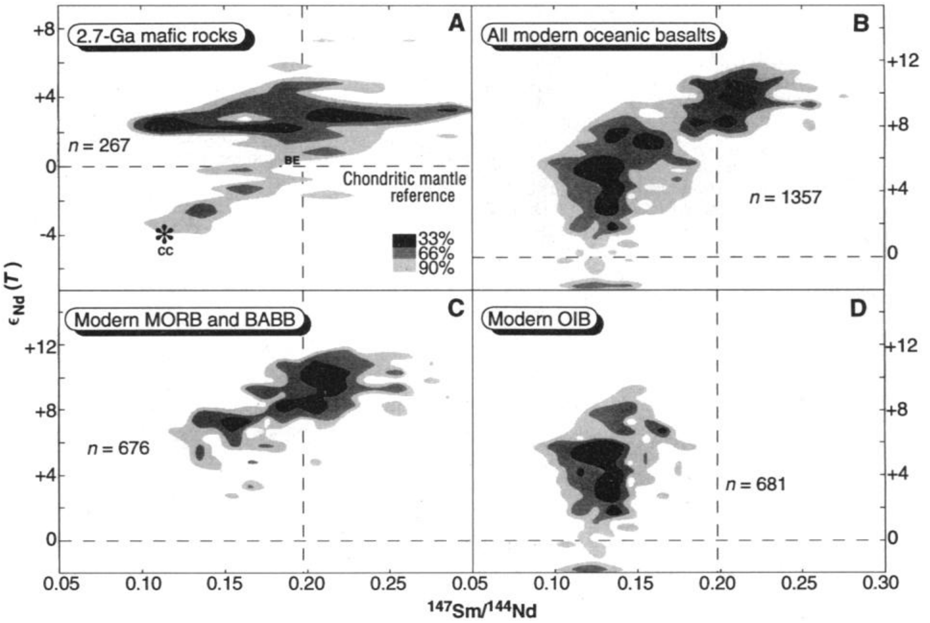

Fig. 1. Density diagrams (proportion of samples) showing the variation in the isotopic composition of Nd as a function of the Sm/Nd ratio among (**A**) Late Archean mantle-derived rocks, (**B**) modern oceanic basalts (OIB, MORB, and BABB), (**C**) modern MORB and BABB [subset of (B)], and (**D**) modern OIB [subset of (B)]. Note the different vertical scale for Archean relative to modern samples. BE is bulk earth. CC is average continental crust. The 267 Late Archean samples originate from widely different areas: 40% are from North America (predominantly the Superior Province), 24% are from Australia (Yilgarn and Pilbara), and 12% are from Africa (Zimbabwe and Kaapvaal). The remaining 24% come from China, India, Brazil, and Finland. The density distribution of (A) does not seem to be biased by sample provenance. We corrected the measured Nd isotope compositions using the best estimate of the crystallization age of each sample, as obtained either directly from isotope geochronological studies or, occasionally, from field relations. Specifically, the ages of 54 of the samples are constrained by U-Pb zircon data, and Pb-Pb and Sm-Nd isochrons constrain the ages of 72 and 119 samples, respectively. The 2.7-Ga age of the remaining 22 samples has been ascribed on the basis of the field relations reported in the original literature. The range in age extends from 2.64 to 2.78 Ga. Propagating this range on the $^{143}Nd/^{144}Nd$ ratio at the time of emplacement ensures that errors on $\epsilon_{Nd}(T)$ related to age assignment are less than half an ϵ unit. Errors arising from analytical uncertainties on both the $^{143}Nd/^{144}Nd$ and $^{147}Sm/^{144}Nd$ ratios are of the same magnitude. Data and references for Archean rocks and modern oceanic basalts are available from the authors upon request.

J. Blichert-Toft, Geological Museum, Copenhagen, Denmark, and Ecole Normale Supérieure de Lyon, France.

F. Albarède, Ecole Normale Supérieure de Lyon, France.

extends toward crustal values, indicating that some mafic magmas were contaminated upon emplacement (Fig. 1A). Likewise, the vertical ridge at crustal $^{147}Sm/^{144}Nd$ values for the modern mantle (Fig. 1B) most probably reflects either interaction of mafic magmas with the crust or the presence of recycled crustal material in the source of basalts (*9*). By contrast, the slanting part of the covariation between $\epsilon_{Nd}(T)$ and $^{147}Sm/^{144}Nd$ that extends over a wide range of $^{147}Sm/^{144}Nd$ ratios (0.10 to 0.30) is considered to represent mantle with minimal contribution of crustal component and will hereafter be referred to as the mantle array.

Once one has recognized the similarities between the Archean and modern mantle, the difference stands out. The mode of the Archean mantle array (as given by the broken crest defined by the 33% contour in Fig. 1A) differs dramatically from that of the modern mantle array, varying by only one ϵ unit (from about +2 to about +3) versus at least eight ϵ units today (from +4 to +12) within the same interval of Sm/Nd ratios. Because particularly few Sm/Nd ratios are available for MORB and modern high-Mg basalts (*10*), these groups are underrepresented in Fig. 1B, but the range of $^{143}Nd/^{144}Nd$ in modern basalts actually amounts to more than 10 ϵ units.

The data in Fig. 1A demonstrate that both long-term depleted and enriched mantle reservoirs had developed globally early in Earth history. The comparable range in $^{147}Sm/^{144}Nd$ ratios for the two mantle arrays further suggests that processes that fractionate Nd and Sm in the mantle today also operated in the Archean. Despite these resemblances, the striking difference in isotopic heterogeneity (Fig. 1, A and B) strongly suggests that there are some fundamental differences between the Late Archean and modern mantle. The variety of rock types included in the compilation of the Late Archean mantle and the large range in Sm/Nd ratios dismiss the possibility that this difference could be an artifact of a biased Archean mantle array resulting from incomplete sampling. Because crust-forming processes had been operating since at least 3.8 Ga, time evidently was not the limitation either to the development of isotopic heterogeneities in the Late Archean mantle of a magnitude similar to that of the present. Rather, heterogeneities created in the $^{147}Sm/^{144}Nd$ ratio in the Late Archean apparently did not survive long enough to be recorded in the $^{143}Nd/^{144}Nd$ ratio (Fig. 2).

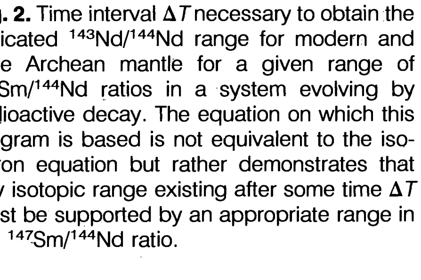

Fig. 2. Time interval ΔT necessary to obtain the indicated $^{143}Nd/^{144}Nd$ range for modern and Late Archean mantle for a given range of $^{147}Sm/^{144}Nd$ ratios in a system evolving by radioactive decay. The equation on which this diagram is based is not equivalent to the isochron equation but rather demonstrates that any isotopic range existing after some time ΔT must be supported by an appropriate range in the $^{147}Sm/^{144}Nd$ ratio.

The linearized equation of radioactive decay over a time interval ΔT can be written

$$\delta\left(\frac{^{147}Sm}{^{144}Nd}\right) \approx \frac{\delta\left(\frac{^{143}Nd}{^{144}Nd}\right)}{\lambda\, \Delta T} \qquad (1)$$

where λ is the decay constant of ^{147}Sm, and $\delta(^{147}Sm/^{144}Nd)$ and $\delta(^{143}Nd/^{144}Nd)$ are the ranges in the $^{147}Sm/^{144}Nd$ ratio and the isotopic composition of Nd, respectively. For the observed variation in $^{143}Nd/^{144}Nd$ of 5×10^{-5} for the Late Archean mantle (Fig. 1A), the lifetime of average heterogeneities in the Sm/Nd ratio on the order of 0.08 was 100 million years (Fig. 2). By contrast, the observed variation in $^{143}Nd/^{144}Nd$ of 5×10^{-4} for the modern mantle (Fig. 1B) indicates that today such heterogeneities survive for 1 billion years (Fig. 2). Conversely, if chemical heterogeneities survived as long in the Late Archean mantle as they do in the mantle today, large differences in the degree of fractionation of the Sm/Nd ratio in the Archean compared with the present are required, an implication that is incompatible with the comparable range of Sm/Nd ratios observed in each of the two environments. We therefore conclude that chemical heterogeneities similar to those observed for the modern mantle also existed in the Late Archean mantle but could not have persisted for longer than one-tenth of the time. This result reinforces other evidence indicating that the secular evolution of Nd isotopes in the Archean mantle was slow from 3.7 to 2.1 Ga (*11*).

The survival time of heterogeneities varies with the difference between the rate of fractionation processes and the rate of convective stirring (mixing time). Because the range in Sm/Nd ratios is similar in the Late Archean and modern mantle, attesting to similar fractionation processes, it is likely that if the survival time was significantly shorter in the Late Archean than it is today, so was the mixing time.

Mixing time is a scale-dependent property that has been parameterized in a number of ways. For single-layer laminar-flow convection, the doubling time, that is the time it takes to stretch a surface by a factor of 2, is proportional to $Ra^{-1/2}$, where Ra is the Rayleigh number (*4*). Therefore, if the doubling time can be scaled by the lifetime of chemical heterogeneities, as inferred above, the Rayleigh number of the Late Archean mantle probably was larger than that of the present-day mantle by two orders of magnitude. A convenient scale for stretching rates is the reciprocal of the velocity gradient. Parameterizing modern mantle convection with plate velocity and mantle depth down to either 670 or 2900 km, depending on whether the mantle is assumed to convect in one or two layers, the time constant associated with the velocity gradient is on the order of 10^8 to 10^9 years, comparable to the lifetime of modern chemical variability. Survival time of heterogeneities an order of magnitude longer today than in the Archean suggests that convective velocities were 10 times greater in the Archean than at present.

Rayleigh number and convective velocity have decreased with time because of the overall decline in heat production. If the above estimates are correct, the present-day thermal regime of the Earth and modern plate tectonics therefore are not directly applicable as analogs for the Archean. Mantle convection at that time probably was considerably more vigorous and unstable, and plumes were perhaps far more numerous than today.

The origin of the $\epsilon_{Nd}(T)$ versus Sm/Nd mantle array and thereby the processes responsible for the bulk of Sm/Nd variability in the mantle source of basalts are not understood. Although continental crust extraction is likely to be responsible for the overall depletion of the mantle in its fertile components, there is little doubt that isotopic heterogeneities within the mantle itself, with the probable exception of the modern recycled component, are not simply associated with crust formation processes. Scaling the survival of heterogeneities by the residence time of mantle Nd relative to material extraction to the crust (*12*) is therefore probably irrelevant.

Other mechanisms that fractionate Sm from Nd in a convecting mantle thus must be considered. Metasomatism by silicate melts produced by small degrees of melting from garnet-bearing assemblages is one way of inducing low Sm/Nd ratios locally in the mantle. Likewise, CO_2-rich liquids—which make up an essential part of fluid inclusions in mantle xenoliths (*13*) and erupt as carbonatite, kimberlite, or melilitite magmas—may also be efficient carriers of incompatible elements (*14*). Alternatively, phase changes induce trace element fractionation across phase boundaries, even in a homogeneous mantle (*15*). At the 670-km boundary that involves garnet and perovskite and potentially separates stable convection levels, substantial Sm/Nd fractionation therefore may take place.

REFERENCES AND NOTES

1. H. E. Huppert, R. S. J. Sparks, J. S. Turner, N. T. Arndt, *Nature* **309**, 19 (1984); H. E. Huppert and R. S. J. Sparks, *Earth Planet. Sci. Lett.* **74**, 371 (1985); N. T. Arndt, *Terra* **6**, 59 (1986).
2. M. Tatsumoto, *Science* **153**, 1094 (1966); P. W. Gast, *Earth Planet. Sci. Lett.* **5**, 353 (1969); C. Brooks, S. R. Hart, A. W. Hofmann, D. E. James, *ibid.* **32**, 51 (1976); R. W. Carlson, J. D. Macdougall, G. W. Lugmair, *Geophys. Res. Lett.* **5**, 229 (1978).
3. F. M. Richter and N. M. Ribe, *Earth Planet. Sci. Lett.* **43**, 212 (1979).
4. N. R. A. Hoffman and D. P. McKenzie, *Geophys. J. R. Astron. Soc.* **82**, 163 (1985).
5. C. J. Allègre, O. Brévart, B. Dupré, J.-F. Minster, *Philos. Trans. R. Soc. London Ser. A* **297**, 447 (1980).
6. G. Schubert and D. Sandwell, *Earth Planet Sci. Lett.* **92**, 234 (1989).
7. W. Abouchami, M. Boher, A. Michard, F. Albarède, *J. Geophys. Res.* **95**, 17605 (1990).
8. J. J. Mahoney, in *Seamounts, Islands, and Atolls*, B. H. Keating, P. Fryer, R. Batiza, G. W. Boehlert, Eds. (Geophys. Monogr. 43, American Geophysical Union, Washington, DC, 1987), p. 207.
9. W. M. White, *Geology* **13**, 115 (1985).
10. B. G. Aitken and L. M. Echeverria, *Contrib. Mineral. Petrol.* **86**, 94 (1984).
11. S. B. Shirey and G. N. Hanson, *Geochim. Cosmochim. Acta* **50**, 2631 (1986).
12. M. Gurnis and G. F. Davies, *J. Geophys. Res.* **91**, 6375 (1986).
13. J. Rosenbaum, A. Zindler, J. L. Rubenstone, *Geochim. Cosmochim. Acta*, in press.
14. D. H. Green and M. E. Wallace, *Nature* **336**, 459 (1988).
15. G. D. Garlick, *Lithos* **2**, 325 (1969); C. R. Bina and M. Kumazawa, *Phys. Earth Planet. Inter.* **76**, 329 (1993).
16. We thank those who reviewed this manuscript at different stages: N. T. Arndt, C. Chauvel, B. Luais, S. B. Shirey, and M. F. Thirlwall. Comments made by two anonymous reviewers greatly improved this manuscript. This is a URA-CNRS 726 contribution.

8 November 1993; accepted 31 January 1994

Growth of Diamond from Atomic Hydrogen and a Supersonic Free Jet of Methyl Radicals

Szetsen Steven Lee, David W. Minsek, Daniel J. Vestyck, Peter Chen*

The growth of small (~10-micrometer) diamond particles (on 0.1- or 0.25-micrometer seed crystals) using an effusive glow discharge nozzle for H$\cdot$ and a separate supersonic pyrolysis jet for $\cdot CH_3$ is reported. Laser micro-Raman, scanning electron microscopy, and x-ray photoelectron spectroscopy data are presented as evidence that well-crystallized diamond is indeed formed. Resonant multiphoton ionization spectroscopy is used as a diagnostic for the gas-phase chemistry indicating that the radical sources are clean and quantitative and that there is no detectable interconversion of $\cdot CH_3$ to C_2H_2 under the conditions of the experiment. Diamond growth is found at substrate temperatures greater than or equal to 650°C with no marked increase in the rate of growth up to 850°C. Acetylene does not give good quality diamond under similar conditions.

The growth of diamond from mixtures of hydrocarbon gases and H_2 on application of some source of energy, for example, thermal filament–assisted chemical vapor deposition (CVD), plasma CVD, and combustion flame CVD, is now an established technology (*1*, *2*). Considerable progress has been made since the early reports of low-pressure growth of polycrystalline diamond films by Derjaguin and co-workers (*3*), Eversole (*4*), and Angus (*5*), with the emphasis now shifting to the rational optimization of growth rates, reduction of defects and nondiamond impurities, and epitaxial growth (*6*) on diamond or nondiamond substrates. To further these ends, there needs to be a better understanding of the basic chemistry of diamond growth, especially with respect to the key atomic and molecular species involved in the growth process.

Mass balance and kinetic considerations have implicated CH_3 and C_2H_2 as the two most likely candidates for the immediate gas-phase precursors to diamond (*7*, *8*). In most systems, an excess of atomic hydrogen has also been found to be necessary. However, in the typical deposition system, as represented by filament-assisted CVD reactors (*2*), the concentrations of reactive species are coupled by gas-phase reactions that proceed as fast as or faster than transport of the species to the growth surface. The separate contribution of each species is difficult to assess and must be inferred from the composite results by indirect methods. Some of these issues are being addressed in fast-flow experiments, that attempt to decouple the separate contributions of different species to the overall growth process (*9*, *10*). Furthermore, the two distinct events of free radical generation in the gas phase and free radical reaction on the surface are also coupled at the relatively high pressures in the typical reactor in such a way that it is difficult to separately optimize each process.

We report the growth of diamond on small diamond seeds under conditions where the hydrocarbon radicals and atomic hydrogen are produced separately and come to interact only at the surface of the growth substrate. A clean, well-characterized, supersonic pyrolysis jet of $\cdot CH_3$ and an effusive glow-discharge jet of H$\cdot$ were separately, but simultaneously, impinged onto a seeded substrate that could be held thermostatically at temperatures from 450° to 900°C. Mixing of the two flows occurs primarily in the region near the surface where the supersonic free jet of $\cdot CH_3$ in helium is disrupted by interaction with the substrate. In this way, the concentrations of reactive species are decoupled from each other and can be independently varied, and the process of radical production is decoupled from the process of surface reaction of the radicals.

Clean, specific generation of $\cdot CH_3$ was done by a continuous-flow version of the supersonic jet flash pyrolysis technique (*11*, *12*). Azomethane, produced by the HgO oxidation of dimethylhydrazine and purified by trap-to-trap distillation, was seeded into 250-torr He (<0.1% seed ratio) and expanded through a heated Al_2O_3 tube nozzle. The terminal 1.0 cm of the 0.6-mm inner diameter tube was heated to ~1000°C by 40-W dc current passing through a molybdenum coil in an annular space between the tube nozzle and another Al_2O_3 jacket. The jacketing was necessary to suppress contamination of the deposition substrate with Mo, which we found to occur for bare coils. We optimized methyl radical production by monitoring the $\cdot CH_3$ concentration using the $3p^2A_2'' \leftarrow X^2A_2''$ transition (*11*, *13*) at 333.4 nm by 2+1 resonant multiphoton ionization (MPI) spectroscopy. We further characterized the methyl radical source by vacuum-ultraviolet photoionization mass spectrometry of the pyrolysate (*14*) using the Nd^{3+}-YAG ninth-harmonic at 118.2 nm. Production of $\cdot CH_3$ from azomethane was found to be clean and quantitative. Under the conditions of the pyrolysis, the ratio $\cdot CH_3/C_2H_2$ was found to be greater than 100:1, with the limit set by the detectability of acetylene by means of the $^1\Delta_g \leftarrow X^1\Sigma_g^+$ origin band (*15*) at 274.9 nm in 2+1 MPI. We estimate the $\cdot CH_3$ flux to be at least 10^{16} radicals per second delivered to a circular spot (at the nozzle-substrate distance) about 0.5 cm in diameter.

S. S. Lee, D. W. Minsek, P. Chen, Mallinckrodt Chemical Laboratory, Harvard University, Cambridge, MA 02138, USA.
D. J. Vestyck, Code 6174, Naval Research Laboratory, Washington, DC 20375, USA.

*To whom correspondence should be addressed.